Elements of Design of Passive Methane Oxidation Biosystems: Fundamental and Practical Considerations about Compaction and Hydraulic Characteristics on Biogas Migration

Geotech Geol Eng (2018) 36:2593–2609
https://doi.org/10.1007/s10706-018-0485-z

Bahar Ahoughalandari[a], Alexandre R. Cabral[a,*] and Serge Leroueil[b]

B. Ahoughalandari · A. R. Cabral (✉)
Geoenvironmental Group, Department of Civil Engineering, University of Sherbrooke, 2500, boul. de l'Université, Sherbrooke, QC J1K 2R1, Canada
e-mail: bahar.ahou@usherbrooke.ca

A. R. Cabral
e-mail: alexandre.cabral@usherbrooke.ca

S. Leroueil
Department of Civil and Water Engineering, Université Laval, Quebec, QC G1K 7P4, Canada
e-mail: serge.leroueil@gci.ulaval.ca

[a] Geoenvironmental Group, Department of Civil Engineering, University of Sherbrooke, Sherbrooke, Quebec, Canada J1K 2R1; bahar.ahou@usherbrooke.ca

[b] Department of Civil and Water Engineering, Université Laval, Quebec, Canada G1K 7P4; serge.leroueil@gci.ulaval.ca

* Corresponding author: Tel.: +1 819 821-7906. Postal address: 2500, boul. de l'Université, Sherbrooke, Quebec, Canada J1K 2R1; alexandre.cabral@usherbrooke.ca

Acknowledgements

This study received financial support from the Natural Science and Engineering Research Council of Canada (NSERC) and Waste Management (WM Quebec Inc.), under the collaborative research and development grant # CRD 379885-08 and from Discovery Grant #170226. The invaluable help of Jean-Guy Lemelin, technician, must also be acknowledged.

Abstract

Passive methane oxidation biosystems (PMOBs) are often proposed as a means to reduce fugitive landfill CH_4 emissions, i.e. emissions not captured by gas collection systems. However, current designs may lead to the formation of a capillary barrier along the interface between the two main layers constituting passive biosystems, namely the methane oxidation layer and gas distribution layer. The formation of a capillary barrier may result in restricted upward flow of biogas at the base of methane oxidation layer, thereby leading to concentrated biogas emissions in regions known as hotpots, where passive oxidation of biotic methane is failing, if not absent. In this study, design criteria are introduced to assess the ease of biogas flow across the gas distribution-methane oxidation layers' interface. Laboratory experiments were conducted to obtain the water retention curve, air permeability function and line of optima (on Standard Proctor curve) of the materials used to construct the methane oxidation layer of two experimental PMOBs at the St-Nicephore (Quebec, Canada) landfill. In addition, the main characteristics for other materials were obtained from the literature. Design criteria were then defined based on the degree of water saturation at the lines of optima and the pattern of air permeability functions and water retention curves. Considering these criteria in the design of PMOBs is fundamental to reduce the risk of creating hotspots when implementing PMOBs.

Keywords: Passive methane oxidation Biosystems; Gas flow behaviour; Capillary barrier effect; Water retention curve; Standard Proctor curve

1 Introduction

Passive methane oxidation biosystems (PMOBs) are considered as cost-effective solutions to reduce fugitive CH_4 emissions, i.e. emissions not captured by gas collection systems (e.g. Cabral et al. 2010b; Capanema and Cabral 2012; He et al. 2012; Huber-Humer et al. 2009; Ndanga et al. 2015; Roncato and Cabral 2012; Scheutz et al. 2009). Generally, a PMOB consists of two main layers: the near surface methane oxidation layer, where methanotrophic bacteria oxidize CH_4 into CO_2, and the underlying gas distribution layer, mainly composed of coarse-grained materials. The main function of the gas distribution layer is to intercept fugitive emissions and distribute them as uniformly as possible at the base of the methane oxidation layer, as illustrated schematically in Fig. 1.

The methane oxidation rate of PMOBs depends on several environmental and operational conditions, including the uniformity of the CH_4 loading (upward flow of fugitive biogas) at the base of the methane oxidation layer. Greater uniformity facilitates the work of methanotrophic bacteria, which results in greater CH_4 oxidation rates (Cabral et al. 2010a; Fredenslund et al. 2010; Scheutz et al. 2011).

The contrast between the unsaturated hydraulic properties of the constituent materials forming the gas distribution and methane oxidation layers leads to the formation of a capillary barrier along their interface, which leads to moisture accumulation, i.e. an increasing degree of water saturation along the interface between gas distribution and methane oxidation layers, from the top to the bottom of the slope. Since degree of water saturation is a key parameter controlling gas flow behaviour through unsaturated soils, the upward migration of fugitive biogas may be diverted within the gas distribution layer towards the drier (upslope) parts of the biosystem. This may eventually lead to the creation of a

hotspot, i.e. a region of high CH_4 fluxes (Bohn and Jager 2011; Cabral et al. 2010a; Röwer et al. 2012) and surface CH_4 concentrations that can be higher than acceptable by legislation.

Several environmental and biological aspects of methane oxidation in PMOBs have been well documented in the technical literature (Ait-Benichou et al. 2009; Capanema and Cabral 2012; Chi et al. 2012; Einola et al. 2007; Gebert et al. 2011; He et al. 2012; Huber-Humer et al. 2009; Ndanga et al. 2015; Roncato and Cabral 2012; Scheutz et al. 2011; Tate 2015). Likewise, the literature abounds with studies that document and analyze air flow through unsaturated soils (Blackwell et al. 1990; Fredlund and Rahardjo 1993; Fredlund et al. 2012; Lu and Likos 2004; Vaughan 2003), the influence of water content on the coefficient of air permeability (Jucá and Maciel 2006; Langfelder et al. 1968; Maciel and Jucá 2000; Marinho et al. 2001; Springer et al. 1998; Tang et al. 2011), and the design of oxygen barriers to prevent acid mine drainage (Bussière et al. 2003; Cabral et al. 2000; Maqsoud et al. 2011; Mbonimpa et al. 2003; Yanful 1993).

On the other hand, very little has been published about the effects of capillary barriers on CH_4 oxidation. For example, Tétreault et al. (2013) conducted a series of numerical simulations to assess the behaviour of two sloped PMOBs whose methane oxidation and gas distribution layers formed capillary barriers. Their results showed that moisture content values were high all along the interfaces, which explained the concentrated biogas fluxes usually found near the top of the two large-scale experimental plots. This behaviour was also observed by Berger et al. (2005), who constructed and monitored the behaviour of an inclined PMOB in the laboratory. In order to minimize the pore obstruction by water associated with the capillary barrier effect, Cassini et al. (2017) constructed an experimental PMOB with a jagged ("zig-zag shape") interface between gas distribution and methane oxidation layers. With this very innovative concept, the pores in methane oxidation layer close to the interface and near every crest would be dry enough to allow unrestricted upward flow of biogas.

Despite the fact that various field experiments have been presented in the technical literature, proper design criteria for PMOBs - taking into consideration the capillary barrier effect and its consequences on upward biogas flow - are still lacking. The purpose of such criteria would be to construct PMOBs with the longest possible length along the interface between the gas distribution and methane oxidation layers where upward gas migration is unrestricted. This length is referred herein as the *length of unrestricted gas migration* (LUGM) It is the only design criterion considered herein.

Samples from the methane oxidation layers of two experimental PMOBs constructed at the St-Nicephore (Quebec, Canada) landfill were analyzed in the laboratory in order to determine their main geotechnical parameters and subsequently to assess gas flow under unsaturated conditions at various initial dry density and water content values. A design parameter, namely the volumetric content at occlusion (θ_{a_occ}), associated with the design criterion LUGM, is proposed (see also Ahoughalandari and Cabral 2016). Its determination can be achieved using simple geotechnical tools, such as the water retention curve and compaction (Standard Proctor) curve. Ultimately, design steps are proposed based on the use of the line of optima of the compaction curve, alone or combined with the water retention curve and air permeability function, when the latter two are available.

The main limitation of the proposed methodology to obtain the fundamental parameters used in the design of PMOBs is associated with the limited number of materials actually characterized in order to develop design parameter. However, the methodology was also applied to materials whose main characteristics were obtained from the literature.

Fig. 1 Schematic layout of a passive methane oxidation biosystem

2 Materials and Methods

2.1 Materials

The material used to construct the methane oxidation layer of the first experimental PMOB was a mixture of five volumes of compost and one volume of coarse sand (D_{10} = 0.07mm, D_{85} = 0.8mm, and the coefficient of uniformity (C_u) = 4.3) with the following characteristics: organic matter content (f_{OC}) equal to 17.8% $g_{o\text{-}m}/g_{dry\text{-}soil}$; specific gravity ($G_s$) equal to 2.24; optimum water content (w_{opt}) and maximum dry density ($\rho_{d\text{-}max}$) equal to 43% and 1080 kg/m^3, respectively (Standard Proctor). The methane oxidation layer of the second PMOB was constituted of uniform sand (D_{50} = 0.15mm and C_u = 2.25) with G_s = 2.71, w_{opt} ~ 12.0%, $\rho_{d\text{-}max}$ = 1750 kg/m^3.

The sand-compost mixture has been reported to show high methane oxidation capacity both in laboratory and field conditions (Cabral et al. 2010b; Roncato and Cabral 2012). The fine sand was selected by Ndanga et al. (2015) to be used in a multi-layer methane oxidation layer that showed very high methane oxidation rate both in laboratory-scale column experiments and in the field.

2.2 Testing

The Standard Proctor test for both materials was performed according to ASTM-D698 (2012). Several test points were chosen to obtain the water retention curve and coefficient of air permeability, k_a (m/s), of the materials for a wide range of initial dry density and water content values (circles in Fig. 2). The compaction effort and method to prepare samples to determine the water retention curve and k_a were different from those used to obtain the compaction curve (Standard Proctor).

Fig. 2 Standard Proctor curves and test points of (a) fine sand, and (b) sand-compost mixture

Test points to determine k_a and water retention curve were selected along 3 constant initial dry density paths (1550 kg/m^3, 1650 kg/m^3 and 1750 kg/m^3) for the fine sand. In the case of the sand-compost mixture, the test points were selected as follows: 4 initial water content and initial dry density values superimposing the Standard Proctor curve (herein denominated "Proctor path") and 3 constant initial dry density paths (750 kg/m^3 (in situ value), 900 kg/m^3 and 1000 kg/m^3). Samples with the required amount of water were kept in plastic bags for at least 48 hours before testing to allow the homogenization of moisture.

2.1.1 Water Retention Curve

The water retention curves were obtained using the modular laboratory instrument HYPROP (UMS GmbH) and following its manual (UMS 2013). With this instrument, it is possible to determine the water retention curve (drying path) of a vertical soil column based on the evaporation method proposed by Wind (1968).

2.1.2 Coefficient of Air Permeability

The coefficient of air permeability (k_a) was measured using a soap flow meter connected to the inlet of an adapted triaxial cell (see schematic as insert in Fig. 4). Each sample was compacted in a membrane surrounded by a rigid mold adapted to the triaxial cell. This mold is equipped with two holes on both sides, through which vacuum is applied during sample preparation. The application of vacuum through these holes ensures that the flexible

membrane sticks adequately to the mold and to the sample, thereby preventing air from flowing between the membrane and the sample. Once the sample preparation is completed, vacuum application is discontinued, but the mold remains in place. The mold was found to be an excellent substitute for the required confining pressure during the air permeability experiments. Several tests were performed to verify this assertion. In order to avoid any air leakage, both ends of the sample were sealed with two O-rings.

Finally, the k_a for each test point (circles in Fig. 2) was calculated for differential air pressure values ranging from 0.5 to 5.0 kPa, in increments of 0.5 kPa, as follows:

$$k_a = \frac{2 \times Q \times \mu \times \Delta x \times P_s \times g}{(P_e^2 - P_s^2) \times A \times \nu} \qquad (1)$$

where P_s (Pa) is the absolute outlet air pressure, P_e (Pa) is the absolute inlet air pressure, Q is the volumetric air flow rate (m^3/s), A is the cross-sectional area of the sample (m^2), Δx is the sample's height (m), g is the acceleration of gravity (m/s^2), μ is the dynamic viscosity of air at ambient temperature (Pa.s), and ν is the kinematic viscosity of air at ambient temperature (m^2/s).

In addition, the gas intrinsic permeability (m^2) of the porous medium, which is independent of the nature of the migrating gas, was calculated as follows:

$$K = \frac{k_a \times \nu}{g} \qquad (2)$$

3 Results

3.1 Fine Sand

Fig. 3 presents the water retention curves of fine sand samples at each of the three values of initial dry density (Fig. 2a) and two initial water content values: one on the dry and the other on the wet side of the line of optima. Water retention curves of the remaining test points (circles in Fig. 2a) led to results quite similar to those shown in Fig. 3 and are therefore not presented. As can be observed, for all initial dry density values in Fig. 3, the air entry values of the sand are easily identifiable: they correspond to the suction values where the samples start to desaturate abruptly. It is noteworthy that the samples underwent negligible reduction in degree of water saturation for suction values lower than their respective air entry values. As expected, Fig. 3 shows that the air entry value increases from ~3 kPa to ~5 kPa with the increase in initial dry density value from 1550 kg/m^3 to 1750 kg/m^3. Otherwise, air entry values for this material are approximately the same for both the dry and wet sides of optima.

Fig. 3 Water retention curves of fine sand samples at two initial water content values (one dry and the other wet of the line of optima) and three different values of initial dry density; (a) 1750 kg/m^3, (b) 1650 kg/m^3 and (c) 1550 kg/m^3

Fig. 4 Variations in the coefficient of air permeability of fine sand with volumetric air content (θ_a), at several values of differential pressure

The relationship between the measured coefficient of air permeability and volumetric air content, herein denominated k_a-function, is presented in Fig. 4 for the three values of initial

dry density. Volumetric air content (θ_a) is defined as the ratio of the volume of air-filled pores to the total volume of a representative sample of the soil. Each point in Fig. 4 represents the value of k_a obtained at a particular θ_a and differential pressure value. Variations in volumetric air content (θ_a) are attributed to the simultaneous changes in initial dry density and water content of the sample. It is not clearly visible in the plot, but several data points corresponding to several values of differential pressure nearly coincide, indicating that the magnitude of the differential air pressure had a minor effect on the k_a value of the compacted samples tested.

Fig. 4 shows that the logarithm of the coefficient of air permeability (k_a) decreases steadily between θ_a = 25% and ~9%. However, in the region indicated by an ellipse in Fig. 4, i.e. when $\theta_a \sim 9\%$, the pattern of decrease in k_a changes, with small decreases in θ_a leading to much more important decreases in k_a. The value of θ_a associated with this change in pattern is denominated herein "occlusion value", or $\theta_{a\text{-}occ}$. In the particular case of Fig. 4, $\theta_{a\text{-}occ} \approx 9\%$, which is in fact the practical threshold of detectable air flow during the experiments. This value corresponds to the degree of water saturation between 70% and 75%. The latter values are greater than the degree of water saturation associated with the line of optima (55%-60%; Fig. 2a). Therefore, what defines the point of occlusion, i.e. $\theta = \theta_{a\text{-}occ}$, occurred on the wet side of the line of optima.

There is probably a *transition zone* for the region defined by $8.5\% < \theta_a < 11\%$, for which air permeability tests were not performed. In any case, it appears from the shape of the graph that the radius of curvature within this zone would be small.

According to Fig. 4, at a given θ_a, the k_a tends to decrease as the initial dry density increases, but the differences are rather small. For example, the tests singled out by arrows (I) and (II)

227 in Fig. 2a have nearly the same θ_a (≈ 15%), and k_a (~ $4x10^{-7}$ m/s for (I), and ~ $5x10^{-7}$ m/s for
228 (II)).

229 Since the ambient temperature was constant during air permeability tests, Fig. 4 can also
230 represent the pattern of gas intrinsic permeability variations with θ_a. Accordingly, it would be
231 possible to use the data in Fig. 4 to assess the CH_4 flow behaviour, instead of the flow
232 behavior of air.

233

234 **3.2 Sand-compost Mixture**

235

236 **Fig. 5** Water retention curves of sand-compost mixture samples at two initial water content
237 values (dry and wet of optima) and at: (a) Standard Proctor dry densities (about 1000 kg/m^3),
238 and (b) in situ dry density (750 kg/m^3)

239

240 Fig. 5 presents the water retention curves of representative samples of the sand-compost
241 mixture. As the initial dry density value was the same on each initial dry density path, very
242 small differences were observed between water retention curves obtained for the "test
243 points", indicated in Fig. 2b. Therefore, only representative water retention curves are
244 presented in Fig. 5. Both water retention curves in Fig. 5a were obtained with samples
245 prepared at two initial dry density and water content values along the Standard Proctor curve,
246 one on the dry side and the other on the wet side. Those presented in Fig. 5b were obtained
247 with samples compacted to attain 750 kg/m^3, which is the in situ dry density of a PMOB
248 tested at the St-Nicephore landfill.

249 The air entry values are not as well defined as they were for the fine sand. Indeed, degree of
250 water saturation started to decrease gradually for suction values lower than the value
251 associated with the commencement of the desaturation zone. Accordingly, the radii of
252 curvature around the air entry values are bigger than those observed in water retention curves
253 of the fine sand. Air entry values values were ~1 kPa for the samples compacted at initial dry
254 density value equal to 750 kg/m^3 and greater than 4 kPa for initial dry density value ~ 1000
255 kg/m^3.

256

257 **Fig. 6** Variations in coefficient of air permeability of sand-compost mixture with volumetric
258 air content at several differential pressure values

259

260 The air permeability function (k_a-function) of the sand-compost mixture is shown in Fig. 6
261 where, for each test point, the k_a value was also measured at several differential pressure
262 values. As in the previous case, data points corresponding to several values of differential
263 pressure coincide. Since all tests were performed at constant ambient temperature, the plot in
264 Fig. 6 can also represent the pattern of gas intrinsic permeability.

265 The curve in Fig. 6 can be subdivided into three zones, which are delimited by two
266 volumetric air content values. The first one is $\theta_a \approx 5\%$. Below this value the obtainment of the
267 k_a was challenging (the soap bubble inside the flowmeter was nearly immobile) and $\theta_a \approx 5\%$
268 can be considered as the "occlusion value", or $\theta_{a\text{-}occ}$. The second delimiting value is $\theta_a \approx$
269 16%. For lower θ_a values soap bubble movement inside the flowmeter was easily measurable,
270 therefore although the k_a-function is steep, it is not as much as when $\theta_a < 5\%$. In the 3rd zone
271 ($\theta_a > 16\%$) the k_a-function is considerably flatter. A practical nomenclature for this second

delimiting value ($\theta_a \approx 16\%$) is **conservative** occlusion value, or **conservative** $\theta_{a\text{-}occ}$. In the case of the sand-compost, a *transition zone* can therefore be identified between **conservative** $\theta_{a\text{-}occ}$ and $\theta_{a\text{-}occ}$ (ellipse in Fig. 6).

For the sand-compost, **conservative** $\theta_{a\text{-}occ}$ corresponds to the degree of water saturation between 73% and 77%, which is lower than the degree of water saturation associated with the line of optima (~90% in Fig. 2b). $\theta_{a\text{-}occ}$ occurs when the degree of water saturation lies between 91% and 92%, i.e. approximately the degree of water saturation at the line of optima (and the degree of water saturation value associated with air entry value; Fig. 5b).

Springer et al. (1998) also identified 3 zones in the k_a-function obtained following tests with silty sand samples, compacted by dropping and stabbing on a constant dry density path. The first zone was identified as the zone of emergence of air permeability at air entry value. The second was associated with the maximum rate of air permeability variation until the gravitational drainage ceased, and the third was associated with the lowest rate of changes for lower values of volumetric water content (therefore greater values of volumetric air content on a constant dry density path).

4 Discussion

4.1 Relationships between the shapes of the Standard Proctor Curve, water retention curve and air permeability function

The establishment of a relationship between unsaturated gas and water flow has been the focus of several studies. For example, Ball et al. (1988) adapted an exponential relationship between hydraulic conductivity and water-filled porosity to relate the air permeability to the

295 air-filled porosity, and validated it experimentally using samples of silty and clayey loam.
296 Ba-Te et al. (2005) obtained a relationship for the coefficient of air permeability (k_a) as a
297 function of suction, by substituting the fitting equation of the water retention curve by an
298 empirical relationship between k_a and degree of water saturation. They validated this
299 relationship using data sets from Singapore residual soils and Japanese soils. Kamiya et al.
300 (2006) developed an apparatus to measure k_a, degree of water saturation and suction,
301 simultaneously. Their results show a clear similarity between the shapes of water retention
302 curves and curves of k_a versus suction for a river silty sand and three types of sandy soils.
303 Ultimately, such relationships – in fact, the parameters that describe the shape of the curves –
304 may be used to infer the point where pores become occluded ($\theta_{a\text{-}occ}$ and/or **conservative**
305 $\theta_{a\text{-}occ}$). This is an essential step in determining the *length of unrestricted gas migration*
306 (LUGM).

307 Relationships derived for materials tested in this study

308 The relationships between water retention curves, air permeability functions (k_a-functions)
309 and Standard Proctor curves were identified in the cases of the fine sand and sand-compost
310 mixtures tested in this study. For both materials, the shapes of water retention curve in the
311 vicinity of the air entry value (Fig. 3 and Fig. 5) show similarities with the corresponding
312 k_a-functions in the vicinity of $\theta_{a\text{-}occ}$, for fine sand (Fig. 4), and between **conservative** $\theta_{a\text{-}occ}$
313 and $\theta_{a\text{-}occ}$, for sand-compost (Fig. 6).

314 It can be observed that the narrower the horizontal distance between the isolines of the degree
315 of water saturation on the Standard Proctor curves (Fig. 2), the steeper the slope of the
316 desaturation zone in the water retention curves (Fig. 3 and Fig. 5), and the steeper the slope of
317 k_a-functions where $\theta_a > \theta_{a\text{-}occ}$ (fine sand; Fig. 4) or $\theta_a >$ **conservative** $\theta_{a\text{-}occ}$ (sand-compost;
318 Fig. 6). The Standard Proctor curve for the sand-compost mixture (Fig. 2b) spans over a

much greater range of water content values than that of the fine sand (Fig. 2a). Accordingly, the isolines of degree of water saturation are wider apart in the case of sand-compost. On a constant dry density path, from the isoline corresponding to the degree of water saturation at occlusion value for the fine sand (70%-75%: see section 3.1) a reduction of 20% in degree of water saturation corresponded to a meager decrease of ~5% in water content. In the case of the sand-compost mixture the same 20% decrease from the isoline associated with the degree of water saturation at occlusion value (91%-92%: see section 3.2) would lead to ~18% decrease in water content. In practical terms, this means that slight changes in water content in the fine sand may lead to pore occlusion, while the sand-compost mixture requires greater increments in moisture to reach occlusion.

For fine sand, the water retention curve along the slope of the desaturation zone (Fig. 3a,b and c) is considerably steeper than for the sand-compost mixture (Fig. 5a,b). Indeed, a 20% reduction of degree of water saturation corresponds to only 4 kPa increase in suction for fine sand (Fig. 3), but nearly 35 kPa for sand-compost (Fig. 5). When $\theta_a > \theta_{a\_occ}$ or $\theta_a >$ conservative θ_{a_occ}, the slope of the k_a-function is steeper for fine sand. Indeed, a 15% reduction of volumetric air content in fine sand leads to nearly one order of magnitude decrease of k_a, whereas it remains within the same order of magnitude for the sand-compost mixture. It is noteworthy that the slope of the k_a-function reflects the sensitivity of k_a value to changes in volumetric air content (or degree of water saturation under constant dry density conditions).

Relationships derived for materials tested in other studies

Fig. 7 presents the water retention curve of materials tested in several other studies, in addition to representative water retention curves of the fine sand (Fig. 3) and sand-compost

343 (Fig. 5). As can be observed, the air entry values of the landfill cover material (Marinho et al.
344 2001), the clay (Jucá and Maciel 2006) and the silty sand (Springer et al. 1998) are not very
345 well defined, as is the case of the sand-compost tested in this study. The shapes of the water
346 retention curve show that desaturation of these materials occurs gradually, in particular in the
347 region where suction values are lower than those associated with the desaturation zone.
348 Similarly to the fine sand tested in this study, the air entry value of the sand tested by Kamiya
349 et al. (2006) is clearly identified and both materials show abrupt desaturation once the air
350 entry value is attained.

351 The steepest desaturation zone observed in Fig. 7 occurred for the fine sand tested in this
352 study, followed by the sand tested by Kamiya et al. (2006). The steepness of the desaturation
353 zone of the 3 other materials, namely landfill cover (Marinho et al. 2001), silty sand (Springer
354 et al. 1998) and sand-compost (this study) are rather similar, with the least steep being that of
355 the sand-compost. In comparison with other published cases, the soils tested in the present
356 study can be considered as representative of two extremes.

357

358 **Fig. 7** Water retention curves of (a) silty sand adapted from Springer et al. (1998), (b) fine
359 sand (this study), (c) sand adapted from Kamiya et al. (2006), (d) sand-compost (this study),
360 (e) clay (CH) adapted from Jucá and Maciel (2006), and (f) landfill cover material adapted
361 from Marinho et al. (2001)

362

363 **Fig. 8** k_a-functions of materials from other studies, adapted from (a) Springer et al. (1998),
364 (b) Jucá and Maciel (2006), (c) Marinho et al. (2001), and (d) Kamiya et al. (2006)

365

366 Fig. 8 shows the k_a-functions of the materials whose water retention curves were presented in
367 Fig. 7. In all figure, the curves were drawn based on the data published by the respective
368 authors. The specific gravity (G_s) was assumed equal to 2.67 for the cases where the actual
369 value was not available. A simple sensitivity analysis showed that varying G_s within a range
370 that is common for the soils in Fig. 8 (~2.62-2.74) did not affect the results presented and the
371 analyses thereof. For the silty sand in Fig. 8a (Springer et al. 1998), the k_a-function is in the
372 form of gas intrinsic permeability versus volumetric air content, because it was not possible
373 to show it otherwise without making too many additional assumptions. The thick solid line
374 represents the slope of the corresponding k_a-function for volumetric air content values greater
375 than the onset of the abrupt decrease in k_a, as was considered in this study. The slope of
376 k_a-functions of the fine sand (Fig. 4; for $\theta_a > \theta_{a\text{-}occ}$) and sand-compost mixture (Fig. 6; for θ_a
377 > **conservative** $\theta_{a\text{-}occ}$) are represented by a dotted line and a dashed line, respectively.

378 In Fig. 8a and b, a *transition zone* is observed within the region with $8\% < \theta_a < 17\%$ and
379 $5\% < \theta_a < 12\%$, respectively (indicated by an ellipse). Therefore, the **conservative** $\theta_{a\text{-}occ}$
380 would be equal to 12% for the clay and 17% for the silty sand. For the landfill cover, despite
381 the gradual desaturation in the vicinity of its air entry value (Fig. 7), a *transition zone* was not
382 identified in its k_a-function (Fig. 8c). Based on the water retention curve of the sand tested by
383 Kamiya et al. (2006) (Fig. 7), one could expect a k_a-function similar to that found for the fine
384 sand of this study, i.e. a k_a-function without a *transition zone*. It is not clear whether there is a
385 *transition zone* in Fig. 8d, due to the lack of test results in the zone where $10\% < \theta_a < 20\%$.

386 The steepest slope of the curve, where volumetric air content is greater than that given by the
387 onset of the abrupt variations in k_a with volumetric air content, is clearly associated with fine
388 sand, followed by the sand tested by Kamiya et al. (2006) (Fig. 8a), the landfill cover material
389 (Fig. 8c) and the sand-compost, the clay (Fig. 8b), and the silty sand (Fig. 8d). The latter 3

have very similar slopes. The clay sample studied by Jucá and Maciel (2006) seems to be an atypical clay, as far as the slope of the desaturation zone of the water retention curve is concerned. For this material, however, the variation of k_a with volumetric air content is minimal for $\theta_a >$ **conservative** $\theta_{a\text{-}occ}$, therefore, the k_a-function behaves as expected for a clayey material. Despite the similarity between the slope of the desaturation zones in water retention curves of sand-compost of this study and landfill cover material (Marinho et al. 2001), the slope of the k_a-function is slightly steeper for the case of landfill cover material (Marinho et al. 2001) than that associated with sand-compost.

Generally, these results seem to indicate that, with the exception of the landfill cover material, the shape of the water retention curve in the vicinity of the air entry value (Fig. 7) corresponds to the shape of the k_a-function in the vicinity of the onset of abrupt decrease in k_a or within the region with **conservative** $\theta_{a\text{-}occ} < \theta_a < \theta_{a\text{-}occ}$. Moreover, a steep slope of the desaturation zone of the water retention curve is associated with a steep slope (thick solid line) of the k_a-function.

Fig. 9 Relationship between the slope of desaturation zones of WRCs and the slope of k_a-functions for $\theta_a > \theta_{a\text{-}occ}$ or $\theta_a >$ **conservative** $\theta_{a\text{-}occ}$, for materials from other studies and this study

For all the materials presented in Fig. 7, except for the clay studied by Jucá and Maciel (2006), calculations were made to determine the absolute value of the slope of the best fitting line for the desaturation zones of the water retention curves and k_a-functions, for volumetric air content values greater than those at the onset of the abrupt decrease in k_a value. The results of these calculations, shown in Fig. 9, are quantitatively consistent with the

414 discussions about Fig. 7 and Fig. 8. Indeed, it is possible to observe a clear trend in the
415 relationship between the slopes of the k_a-function and water retention curve: the greater the
416 slope of water retention curve, the greater the slope of k_a-function.

417

418 **Fig. 10** Compaction curves of (a) fine sand (this study), (b) Landfill cover material adapted
419 from Marinho et al. (2001), (c) MH-CH adapted from Langfelder et al. (1968), and (d)
420 sand-compost (this study)

421

422 Fig. 10 presents the Standard Proctor curves of the materials tested in this and in other studies
423 found in the technical literature. For sake of comparison, the horizontal distances between
424 isolines of degree of water saturation 20% apart (represented by arrows in Fig. 10) were
425 measured for a dry density value 200 kg/m^3 lower than the optimum dry density. This
426 arbitrary value was chosen so that the arrows are of identifiable enough dimensions in the
427 figure. The shortest distance is associated with the fine sand (this study), followed by the
428 landfill cover material (Marinho et al. 2001), the MH-CH (Langfelder et al. 1968) and
429 sand-compost (this study).

430

431 **Fig. 11** The k_a-function of the MH-CH material adapted from Langfelder et al. (1968),
432 accompanied by materials tested in this study

433

434 This same order above is observed when the slope of the k_a-functions of the same materials
435 are compared. Indeed, as can be observed in Fig. 11, the steepest slope is associated with the
436 k_a-function of the fine sand, followed by the MH-CH (Langfelder et al. 1968) and the

437 sand-compost. Based on this limited amount of data, it is tempting to state that the shorter the
438 distance between isolines of degree of water saturation, the steeper the slope of the
439 k_a-function. However, as indicated in Fig. 11, the slope of the k_a-function of the landfill cover
440 (Marinho et al. 2001) is slightly less steep than that of the MH-CH (Langfelder et al. 1968),
441 despite the fact that the distance between isolines of degree of water saturation is slightly
442 shorter for the landfill cover material.

443 It is well known that the slope of the desaturation zone of water retention curves of
444 fine-grained soils is less steep than in the case of coarse-grained soils, while compaction
445 curves of fine-grained materials spread over a wider range of water content values than the
446 compaction curves of coarse-grained materials.

447 Considering the above discussion, valuable information about gas flow behavior through
448 PMOBs can thus be extracted from examination of the shapes of the compaction curve, and
449 the water retention curve. In other words, critical design steps can be accomplished using
450 simple and easy-to-obtain data, such as compaction curves and water retention curve.

451

452 **4.2 Relationships between degree of water saturation associated with occlusion value**
453 **and degree of water saturation at the line of optima and at air entry value**

454 Results of air permeability tests obtained by Langfelder et al. (1968) with clay or silty
455 samples compacted dynamically (Standard Proctor and other), statically or by kneading,
456 show that close to the optimum water content, slight increases in water content cause several
457 orders of magnitude reduction in the k_a value. Similar findings were obtained by Marinho et
458 al. (2001) and Jucá and Maciel (2006) who tested silty samples. According to Leroueil and
459 Hight (2013), the pores of soils compacted on the wet side of optimum are occluded, i.e. the
460 air-phase is in the form of discontinuous bubbles, whereas the air phase is continuous on the

461 dry side of optimum. All this seems to indicate that occlusion occurs near optimum water
462 content. This was also observed in the case of the sand-compost mixture, where the degree of
463 water saturation at the line of optima coincides with occlusion of air pores (see discussion in
464 section 3.2). For the fine sand, however, the degree of water saturation associated with
465 occlusion value is greater than that given by the line of optima (see section 3.1).

466 In addition, according to the k_a-function (Fig. 6) and water retention curves (Fig. 5) of the
467 sand-compost mixture, the degree of water saturation associated with the air entry value
468 provided a reasonable estimate of degree of water saturation at pore occlusion. In the case of
469 fine sand, the degree of water saturation at air entry value (Fig. 3) would not be a good
470 indicator of occlusion, because the pores would be occluded at a degree of water saturation
471 lower than that associated with the air entry value (see section 3.1).The abrupt decrease of
472 coefficient of air permeability values with decreasing suction (therefore with increasing
473 degree of water saturation), for suction values lower than the air entry value, has been
474 reported in the literature (e.g. Fredlund et al. 2012). However, in certain cases, the abrupt
475 decrease in coefficient of air permeability that characterizes occlusion begins at a degree of
476 water saturation value lower than that associated with air entry value (Kamiya et al.
477 2006).This seems to indicate that further investigation is required in order to find a more
478 precise indicator of pore occlusion based on water retention curve.

479

480 **4.3 Design Steps**

481 The above discussion shows that easily available data (such as the Standard Proctor curve
482 and/or water retention curve) can be used to infer the shape of k_a-function and, eventually the
483 degree of water saturation associated with $\theta_{a\text{-}occ}$ (or with **conservative** $\theta_{a\text{-}occ}$). Ultimately, this

484 information can be used to obtain the design parameters required to determine the length of
485 *unrestricted gas migration* (LUGM).

486 For methane oxidation layers constituted of materials similar to the fine sand biogas can flow
487 unrestricted across the interface between gas distribution and methane oxidation layers, as
488 long as the volumetric air content remains greater than occlusion value. The latter is to be
489 obtained in the manner explained in the remainder of this section. LUGM would be the length
490 of the interface between the methane oxidation and gas distribution layers, taken horizontally,
491 along which θ_a is greater than $\theta_{a\text{-}occ}$ of methane oxidation layer material. In the case of
492 methane oxidation layers constructed with materials similar to the sand-compost mixture, gas
493 flow would be considered reasonably unrestricted beyond the point along the interface where
494 θ_a becomes lower than **conservative** $\theta_{a\text{-}occ}$.

495 The occlusion or **conservative** occlusion values would be obtained as follows:

496 a) If the k_a-function is available, the occlusion value is defined as the volumetric air
497 content at which the soap bubble inside the flowmeter is nearly immobile. It is arbitrary, but
498 it is nonetheless a practical definition. In cases where the **conservative** occlusion value can
499 be identified via the k_a-function (e.g. sand-compost mixture; Fig. 6), using the **conservative**
500 occlusion value to define the occlusion and to calculate LUGM leads to a conservative
501 design.
502 b) In the absence of the k_a-function, for methane oxidation layer materials that behave in
503 a manner similar to the fine sand, one can resort to the degree of water saturation
504 corresponding to the line of optima (of the Standard Proctor) to calculate the occlusion value
505 and LUGM. A certain level of conservatism is imbedded in this approach.
506 c) In the absence of the k_a-function, for materials that behave in a similar manner to the
507 sand-compost mixture (i.e. air entry value not well defined), using the degree of water

saturation 10% to 20% lower than that corresponding to the line of optima, i.e. degree of water saturation at optima minus 10% to 20%, would lead to volumetric air contents in the vicinity of **conservative** $\theta_{a\text{-}occ}$. This ensures at least viable biogas migration. LUGM would be therefore defined based on **conservative** $\theta_{a\text{-}occ}$.

This arbitrary selection in c above was verified based on the results presented by Maciel and Jucá (2000) on sandy clay samples, for which the difference between the degree of water saturation at the start and end of what has been defined herein as the *transition zone*, i.e. **conservative** $\theta_{a\text{-}occ} > \theta_a > \theta_{a\text{-}occ}$ (see for example, Fig. 6) was approximately 20%. Likewise, Springer et al. (1998) and Ba-Te et al. (2005) reported nearly 14% and 13% changes in volumetric water content within the *transition zone* for a silty sand and for Japanese fine soils, respectively. Here again, more refined design procedures will eventually be developed with further studies concerned with the hydraulic behaviour of PMOBs.

4.4 Further design considerations

As discussed in section 4.1, the slope of k_a-functions where $\theta_a > \theta_{a\text{-}occ}$ (fine sand) or $\theta_a >$ **conservative** $\theta_{a\text{-}occ}$ (sand-compost) corresponds to the slope of the desaturation zone in the water retention curves. It is therefore possible to use the slope of the desaturation zone of the water retention curve - or the slope of k_a-function where θ_a is greater than occlusion or **conservative** occlusion value - to help in the selection of the methane oxidation layer material. Shallower slopes of the curves lead to greater uniformity of volumetric air content and degree of water saturation along the interface between methane oxidation and gas distribution layers. This greater uniformity leads more efficient biogas distribution at the base of the methane oxidation layer.

5 Conclusions

In this study a key criterion for designing passive methane oxidation biosystems, denominated *length of unrestricted gas migration* (LUGM) was defined, and steps to obtain the parameters needed to determine it, were presented. These parameters, i.e. θ_a and **conservative** $\theta_{a\text{-}occ}$, were defined as the threshold of unrestricted upward flow of biogas. The flow of biogas was considered reasonably unrestricted when: 1) $\theta_a > \theta_{a\text{-}occ}$ for methane oxidation layer materials similar to the fine sand tested in this study, and 2) when $\theta_a >$ **conservative** $\theta_{a\text{-}occ}$ for methane oxidation layer materials similar to the sand-compost mixture.

Similarities were found between the shapes of air permeability function around $\theta_{a\text{-}occ}$ (and/or **conservative** $\theta_{a\text{-}occ}$) and water retention curve around the air entry value, as well as between the width over which the Standard Proctor curve spans and the slope of air permeability function and water retention curve. It was also shown that in the absence of air permeability function, one can resort to the degree of water saturation at the line of optima or degree of water saturation at air entry value to obtain the value of $\theta_{a\text{-}occ}$ and/or **conservative** $\theta_{a\text{-}occ}$. The methodology presented to obtain $\theta_{a\text{-}occ}$ and **conservative** $\theta_{a\text{-}occ}$ helps in the selection of the appropriate material for methane oxidation leyer. One that would provide the longest possible LUGM, therefore the lowest risk of hotspot creation.

References

Ahoughalandari, B., and Cabral, A.R. 2016. Influence of capillary barrier effect on biogas distribution at the base of passive methane oxidation biosystems: Parametric study. doi: 10.1016/j.wasman.2016.11.026.

555 Ait-Benichou, S., Jugnia, L.-B., Greer, C.W., and Cabral, A.R. 2009. Methanotrophs and
556 Methanotrophic Activity in Engineered Landfill Biocovers. Waste Management **29**(9): 2509-
557 2517.
558 ASTM-D698. 2012. Standard Test Methods for Laboratory Compaction Characteristics of Soil
559 Using Standard Effort (12,400 ft-lbf/ft3 (600 kN-m/m3)). ASTM International, West
560 Conshohocken, PA.
561 Ba-Te, Zhang, L., and Fredlund, D. 2005. A General Air-phase Permeability Function for
562 Airflow through Unsaturated Soils. *In* Slopes and Retaining Structures Under Seismic and
563 Static Conditions. pp. 1-15.
564 Ball, B.C., O'Sullivan, M.F., and Hunter, R. 1988. Gas Diffusion, Fluid Flow and Derived Pore
565 Continuity Indices in Relation to Vehicle Traffic and Tillage. Journal of Soil Science **39**: 327-
566 339.
567 Berger, J., Fornés, L.V., Ott, C., Jager, J., Wawra, B., and Zanke, U. 2005. Methane Oxidation
568 in a Landfill Cover with Capillary Barrier. Waste Management **25**: 369-373.
569 Blackwell, P.S., Ringrose-Voase, A.J., Jayawardane, N.S., Olssons, K.A., Mckenzie, D.C., and
570 Mason, W.K. 1990. The Use of Air-filled Porosity and Intrinsic Permeability to Air to
571 Characterize Structure of Macropore Space and Saturated Hydraulic Conductivity of Clay
572 Soils. Journal of Soil Science **41**: 215-228.
573 Bohn, S., and Jager, J. 2011. Low Gas Emissions of Mechanically and Biologically Treated
574 Waste and Microbial Methane Oxidation as an Adapted Method for Mitigation of Emissions.
575 *In* XIII International Waste Management and Landfill Symposium CISA Publisher S.
576 Margherita di Pula, Italy.
577 Bussière, B., Aubertin, M., and Chapuis, R.P. 2003. The Behavior of Inclined Covers Used as
578 Oxygen Barriers. Canadian Geotechnical Journal **40**: 512-535.

579 Cabral, A., Racine, I., Burnotte, F., and Lefebvre, G. 2000. Diffusion of Oxygen through a Pulp
580 and Paper Residue Barrier. Canadian Geotechnical Journal **37**: 201-217.
581 Cabral, A.R., Létourneau, M., Yanful, E., Song, Q., McCartney, J.S., and Parks, J. 2010a.
582 Geotechnical Issues in the Design and Construction of PMOBs. *In* UNSAT 2010, Barcelona.
583 pp. 1361-1367.
584 Cabral, A.R., Moreina, J.F.V., and Jungia, L.B. 2010b. Biocover Performance of Landfill
585 Methane Oxidation: Experimental Results. Journal of Environmental Engineering **136**: 785-
586 793.
587 Capanema, M.A., and Cabral, A.R. 2012. Evaluating Methane Oxidation Efficiencies in
588 Experimental Landfill Biocovers by Mass Balance and Carbon Stable Isotopes. Water Air Soil
589 Pollut **223**(9): 5623-5635.
590 Cassini, F., Scheutz, C., Skov, B.H., Mou, Z., and Kjeldsen, P. 2017. Mitigation of methane
591 emissions in a pilot-scale biocover system at the AV Miljø Landfill, Denmark: 1. System
592 design and gas distribution. Waste Management. doi:
593 http://dx.doi.org/10.1016/j.wasman.2017.01.013.
594 Chi, Z.F., Lu, W.J., Li, H., and Wang, H.T. 2012. Dynamics of CH_4 Oxidation in Landfill
595 Biocover Soil: Effect of O_2/CH_4 Ratio on CH_4 Metabolism. Environmental Pollution **170**: 8-
596 14.
597 Einola, J.-K.M., Kettunen, R.H., and Rintala, J.A. 2007. Responses of Methane Oxidation to
598 Temperature and Water Content in Cover Soil of a Boreal Landfill. Soil Biology &
599 Biochemistry **39**: 1156-1164.
600 Fredenslund, A.M., Scheutz, C., and Kjeldsen, P. 2010. Tracer Method to Measure Landfill
601 Gas Emissions from Leachate Collection Systems. Waste Management **30**: 2146–2152.
602 Fredlund, D.G., and Rahardjo, H. 1993. Soil Mechanics for Unsaturated Soils. John Wiley &
603 Sons, Inc.

Fredlund, D.G., Rahardjo, H., and Fredlund, M.D. 2012. Unsaturated Soil Mechanics in Engineering Practice. John Wiley & Sons, Inc., Hoboken, NJ, USA. pp. 9.

Gebert, J., Groengroeft, A., and Pfeiffer, E.M. 2011. Relevance of Soil Physical Properties for the Microbial Oxidation of Methane in Landfill Covers. Soil Biol Biochem **43**: 1759-1767.

He, R., Wang, J., Xia, F., Mao, L., and Shen, D. 2012. Evaluation of Methane Oxidation Activity in Waste Biocover Soil During Landfill Stabilization. Chemosphere **89**: 672-679.

Huber-Humer, M., Röder, S., and Lechner, P. 2009. Approaches to Assess Biocover Performance on Landfills. Waste Management **29**: 2092-2104.

Jucá, J., and Maciel, F. 2006. Gas Permeability of a Compacted Soil Used in a Landfill Cover Layer. *In* Fourth International Conference on Unsaturated Soils. *Edited by* G.A. Miller and C.E. Zapata and S.L. Houston and D.G. Fredlund. American Society of Civil Engineers, Carefree, Arizona, United States. pp. 1535-1546.

Kamiya, K., Bakrie, R., and Honjo, Y. 2006. A New Method for the Measurement of Air Permeability Coefficient of Unsaturated Soil. *In* Fourth International Conference on Unsaturated Soils. *Edited by* G.A. Miller and C.E. Zapata and S.L. Houston and D.G. Fredlund. American Society of Civil Engineers, Carefree, Arizona, United States. pp. 1741-1752.

Langfelder, L.J., Chen, C.F., and Justice, J.A. 1968. Air Permeability of Compacted Cohesive Soils. Journal of the Soil Mechanics and Foundations Division **94**(4): 981-1002.

Leroueil, S., and Hight, D.W. 2013. Compacted Soils: From Physics to Hydraulic and Mechanical Behaviour. *In* First Pan-American Conference on Unsaturated Soils. *Edited by* C.M. Bernardo Caicedo, Laureano Hoyos, Julio Esteban Colmenares, Ivan Rafael Berdugo, Cartagena, Colombia. pp. 41-59.

Lu, N., and Likos, W.J. 2004. Unsaturated Soil Mechanics. John Wiley & Sons, Inc. pp. 556.

627 Maciel, F., and Jucá, J. 2000. Laboratory and Field Tests for Studying Gas Flow Through MSW
628 Landfill Cover. *In* Geo-Denver. *Edited by* C.D. Shackelford and S.L. Houston and N.Y. Chang.
629 American Society of Civil Engineers, Denver, Colorado, United States. pp. 569-585.
630 Maqsoud, A., Bussière, B., Aubertin, M., Chouteau, M., and Mbonimpa, M. 2011. Field
631 Investigation of a Suction Break Designed to Control Slope-Induced Desaturation in an
632 Oxygen Barrier. Canadian Geotechnical Journal **48**: 53-71.
633 Marinho, F.A.M., Andrade, M.C.J., and Jucá, J.F.T. 2001. Air and Water Permeability of a
634 Compacted Soil Used in a Solid Waste Landfill in Recife, Brazil. *In* the Third BGA
635 Geoenvironmental Engineering Conference. Thomas Telford Publishing, Thomas Telford Ltd.,
636 Edinburg, Scotland. pp. 437-442.
637 Mbonimpa, M., Aubertin, M., Aachib, M., and Bussière, B. 2003. Diffusion and Consumption
638 of Oxygen in Unsaturated Cover Materials. Canadian Geotechnical Journal **40**: 916-932.
639 Ndanga, É.M., Bradley, R.L., and Cabral, A.R. 2015. Does Vegetation Affect the Methane
640 Oxidation Efficiency of Passive Biosystems? Waste Management **38**: 240-249.
641 Roncato, C.D.L., and Cabral, A.R. 2012. Evaluation of Methane Oxidation Efficiency of Two
642 Biocovers: Field and Laboratory Results. Journal of Environmental Engineering **138**(2): 164-
643 173.
644 Röwer, I.U., Gebert, J., Streese-Kleeberg, J., Kleinschmidt, V., Melchior, S., Scharff, H., and
645 Pfeiffer, E.-M. 2012. Heterogeneous Emission from a Biocover Designed for Methane
646 Oxidation. *In* 7th Intercontinental Landfill Research Symposium (ICLRS). Poster presentation,
647 Luleä, Sweden.
648 Scheutz, C., Fredenslund, A.M., Chanton, J., Pedersen, G.B., and Kjeldsen, P. 2011. Mitigation
649 of Methane Emission from Fakse Landfill Using a Biowindow System. Waste Management
650 **31**: 1018-1028.

651 Scheutz, C., Kjeldsen, P., Bogner, J.E., De Visscher, A., Gebert, J., Hilger, H.A., Huber-
652 Humer, M., and Spokas, K. 2009. Microbial Methane Oxidation Processes and Technologies
653 for Mitigation of Landfill Gas Emissions. Waste Management and Research **27**(5): 409-455.
654 Springer, D.S., Loaiciga, H.A., Cullen, S.J., and Everett, L.G. 1998. Air Permeability of Porous
655 Materials Under Controlled Laboratory Conditions. Groundwater **36**(4): 558-565. doi:
656 10.1111/j.1745-6584.1998.tb02829.x.
657 Tang, A.M., Cui, Y.-J., Richard, G., and Défossez, P. 2011. A Study on the Air Permeability
658 as Affected by Compression of Three French Soils. Geoderma **162**: 171-181.
659 Tate, K.R. 2015. Soil Methane Oxidation and Land-Use Change - from Process to Mitigation.
660 Soil Biology & Biochemistry **80**: 260-272.
661 Tétreault, P., Cabral, A.R., and Abdolahzadeh, A.M. 2013. Non-Uniform Distribution of
662 Biogas under a Biocover due to Capillary Barrier Effect: Case Studies. *In* GEOMontreal,
663 Montreal, Canada.
664 UMS. 2013. HYPROP-UMS User's Manual. *In* Art. no. HYPROP Version 02. UMS GmbH
665 München.
666 Vaughan, P.R. 2003. Observations on the Behaviour of Clay Fill Containing Occluded Air
667 Bubbles. Géotechnique **53**(2): 265-272.
668 Wind, G.P. 1968. Capillary Conductivity Data Estimated by a Simple Method. *In* R.E. Rijtema
669 and H. Wassink (ed.) Water in the Unsaturated Zone: Proc. UNESCO/IASH Symp.,
670 Wageningen, the Netherlands. pp. 181-191.
671 Yanful, E.K. 1993. Oxygen Diffusion through Soil Covers on Sulphidic Mine Tailings. Journal
672 of Geotechnical Engineering **119**(8): 1207-1228.

673

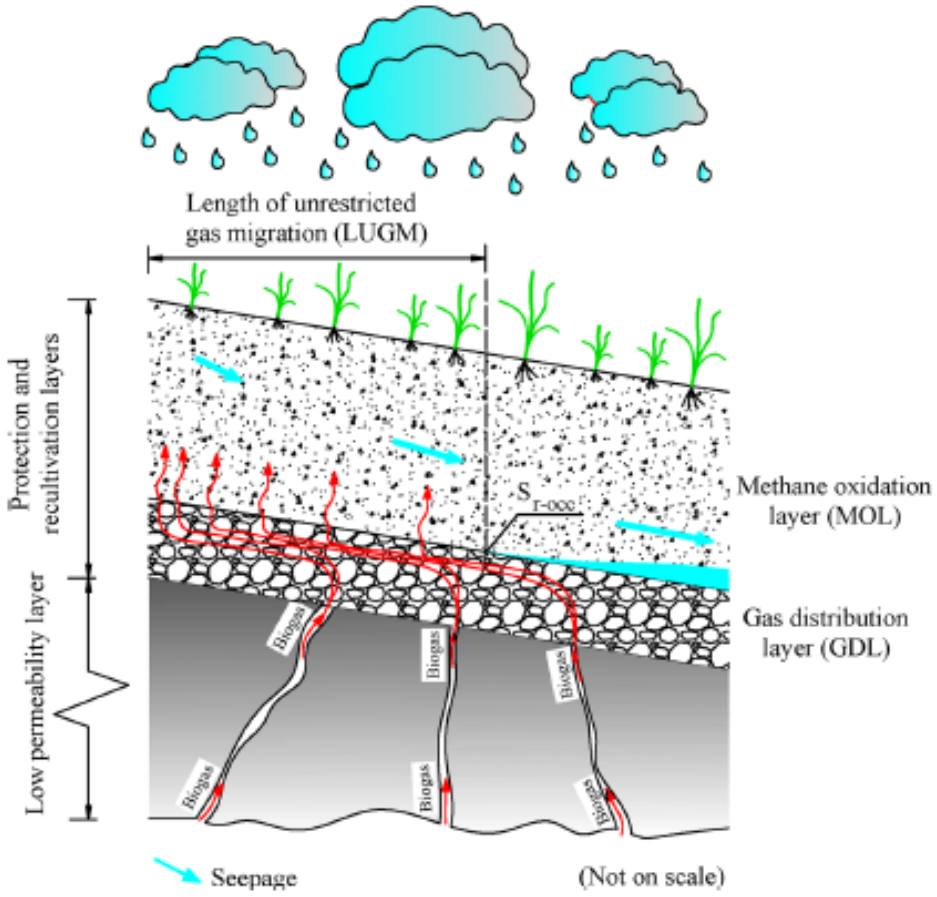

Fig. 1 Schematic layout of a passive methane oxidation biosystem

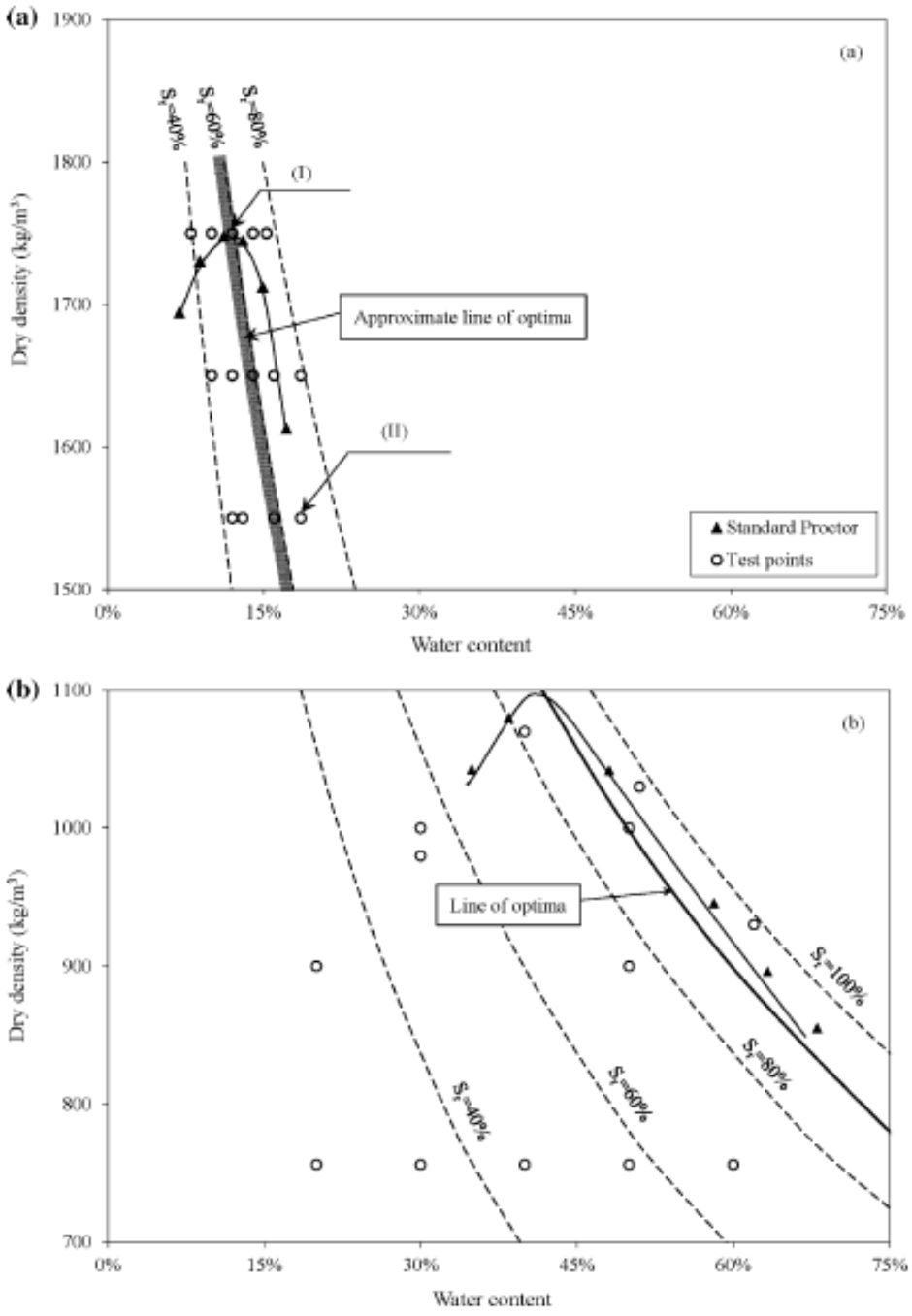

Fig. 2 Standard Proctor curves and test points of (a) fine sand, and (b) sand compost mixture

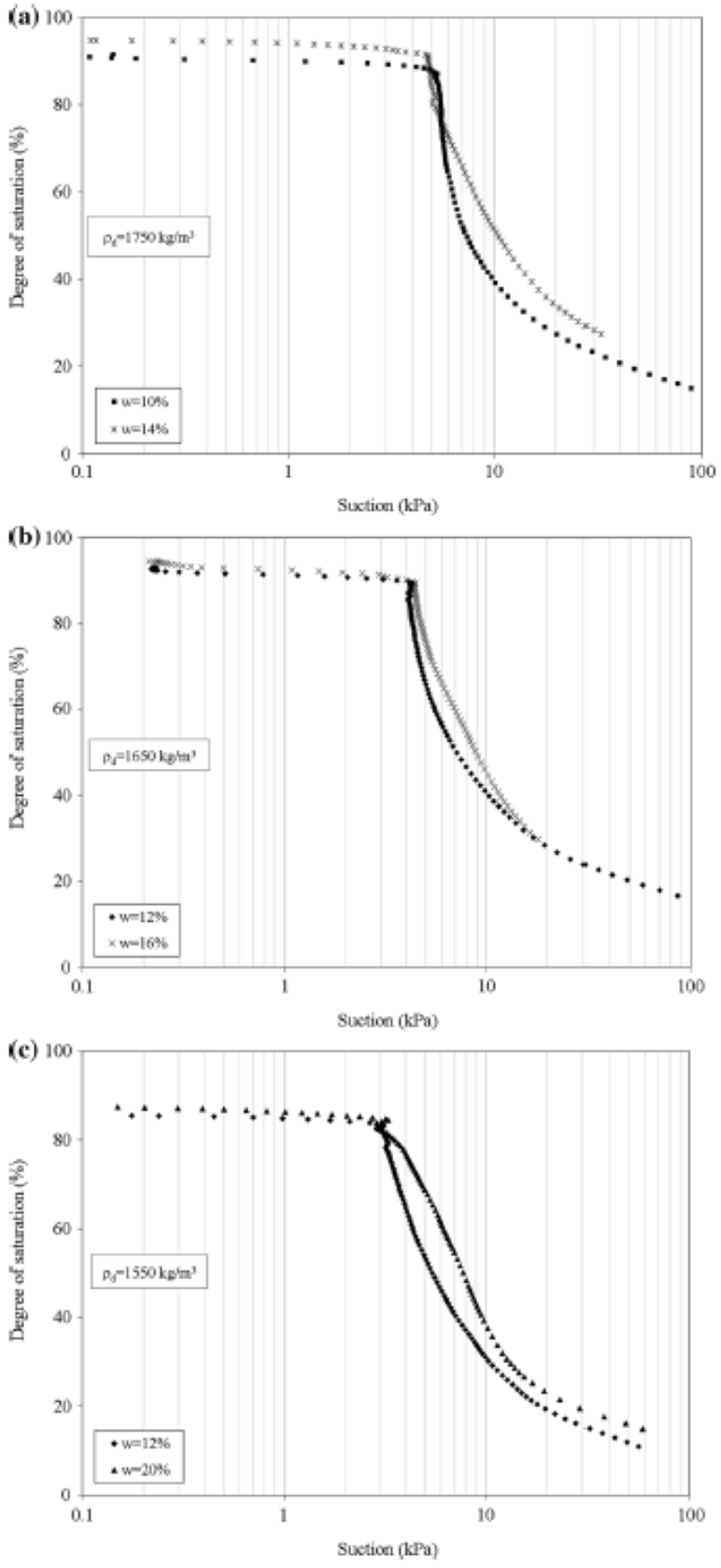

Fig. 3 Water retention curves of fine sand samples at two initial water content values (one dry and the other wet of the line of optima) and three different values of initial dry density; (a) 1750 kg/m3, (b) 1650 kg/m3 and (c) 1550 kg/m3

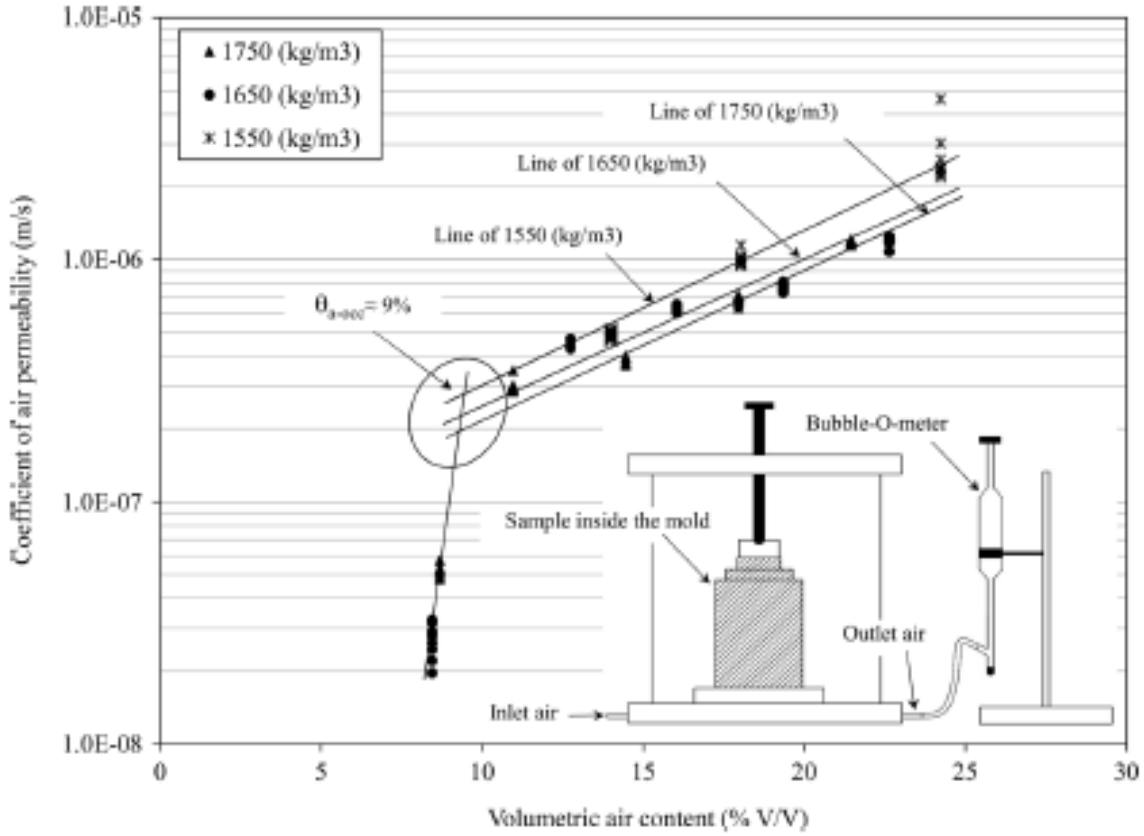

Fig. 4 Variations in the coefficient of air permeability of fine sand with volumetric air content (θ_a), at several values of differential pressure

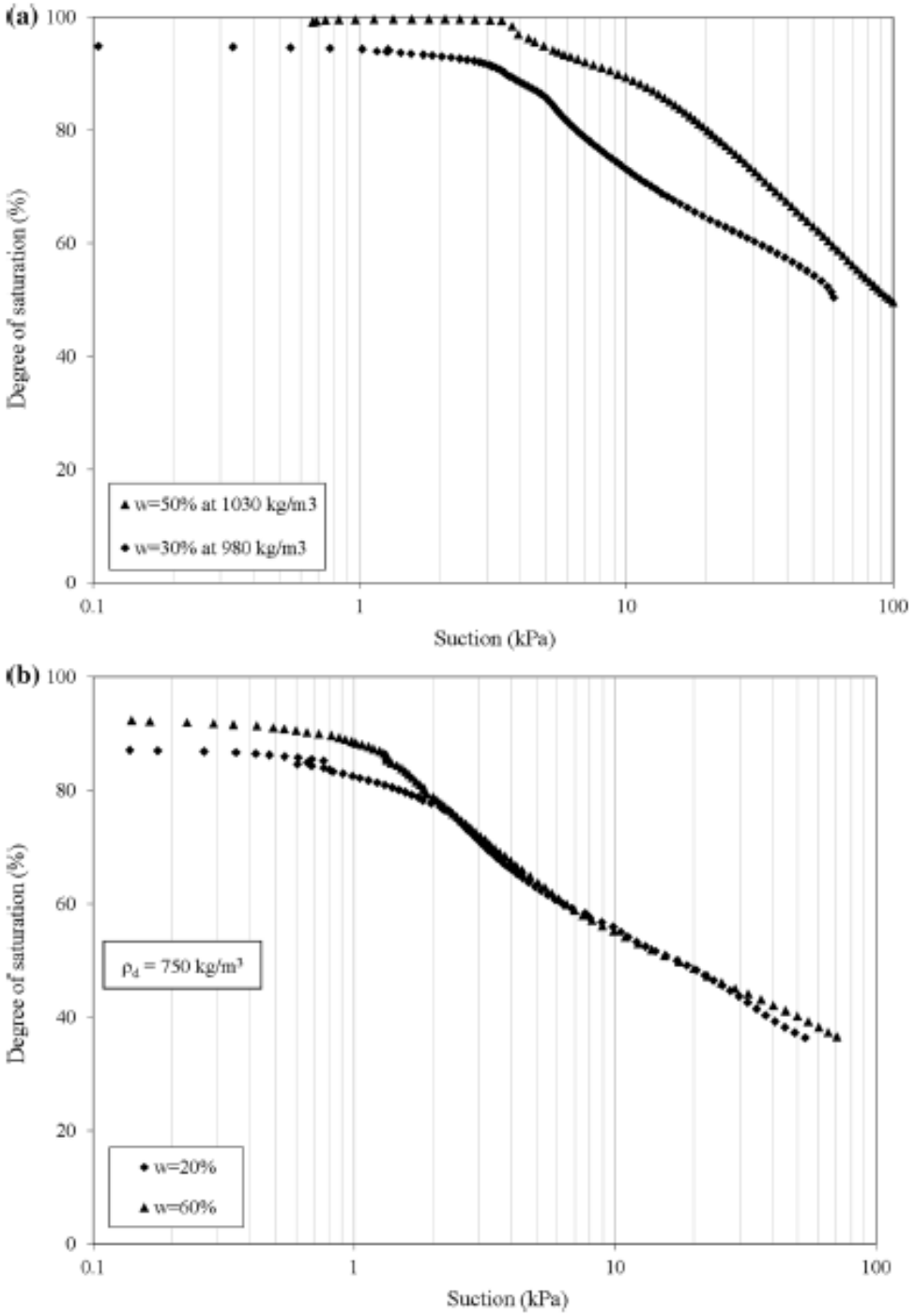

Fig. 5 Water retention curves of sand-compost mixture samples at two initial water content values (dry and wet of optima) and at: (a) Standard Proctor dry densities (about 1000 kg/m^3), and (b) in situ dry density (750 kg/m^3)

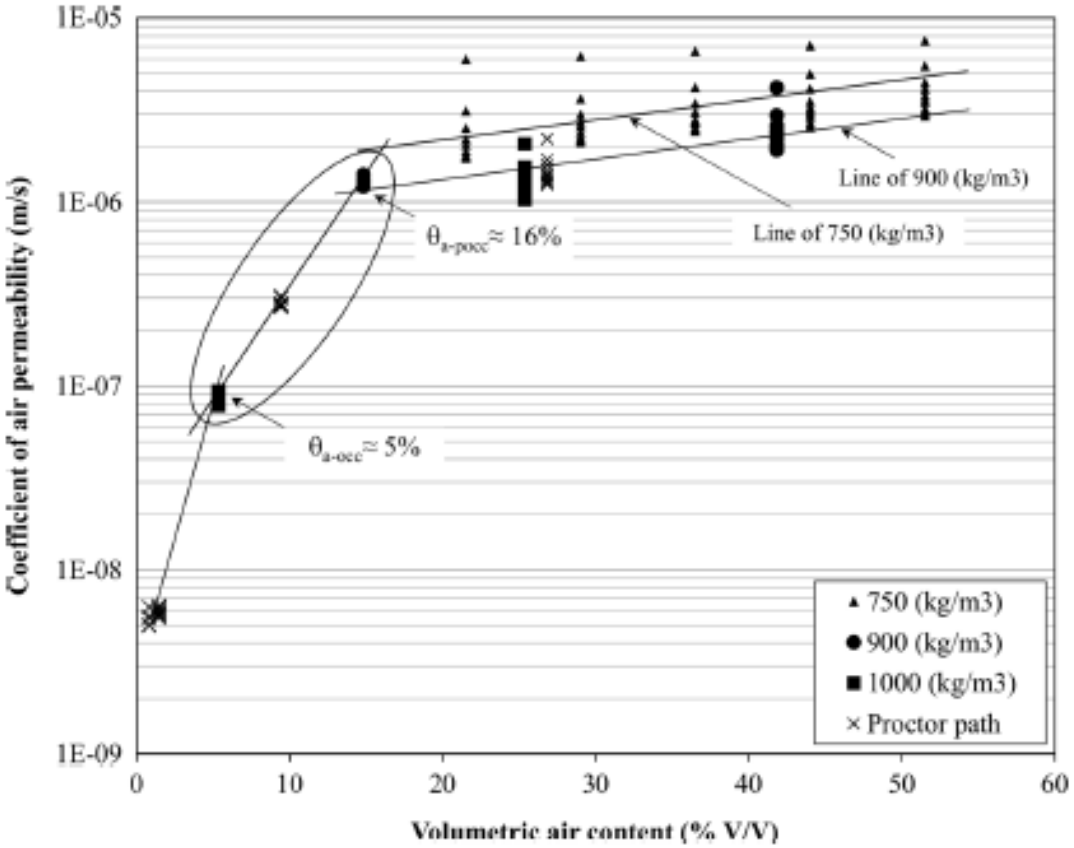

Fig. 6 Variations in coefficient of air permeability of sand-compost mixture with volumetric air content at several differential pressure values

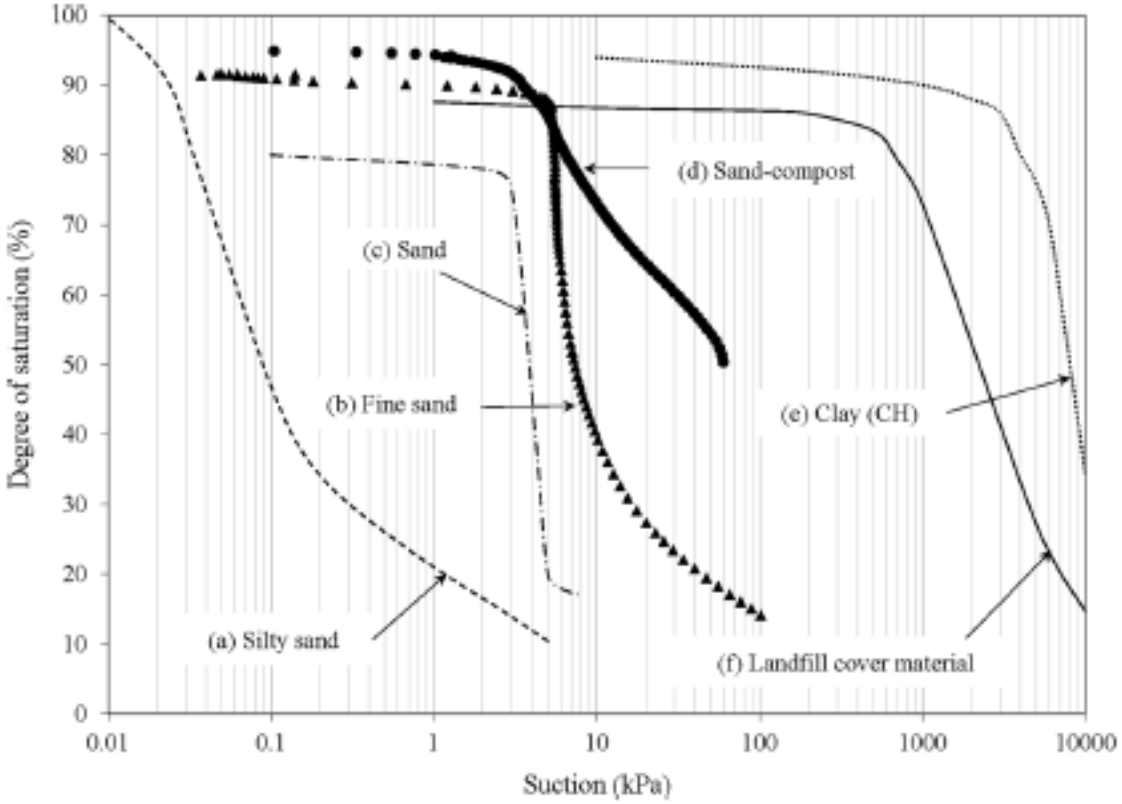

Fig. 7 Water retention curves of (a) silty sand adapted from Springer et al. (1998), (b) fine sand (this study), (c) sand adapted from Kamiya et al. (2006), (d) sand compost (this study), (e) clay (CH) adapted from Jucá and Maciel (2006), and (f) landfill cover material adapted from Marinho et al. (2001)

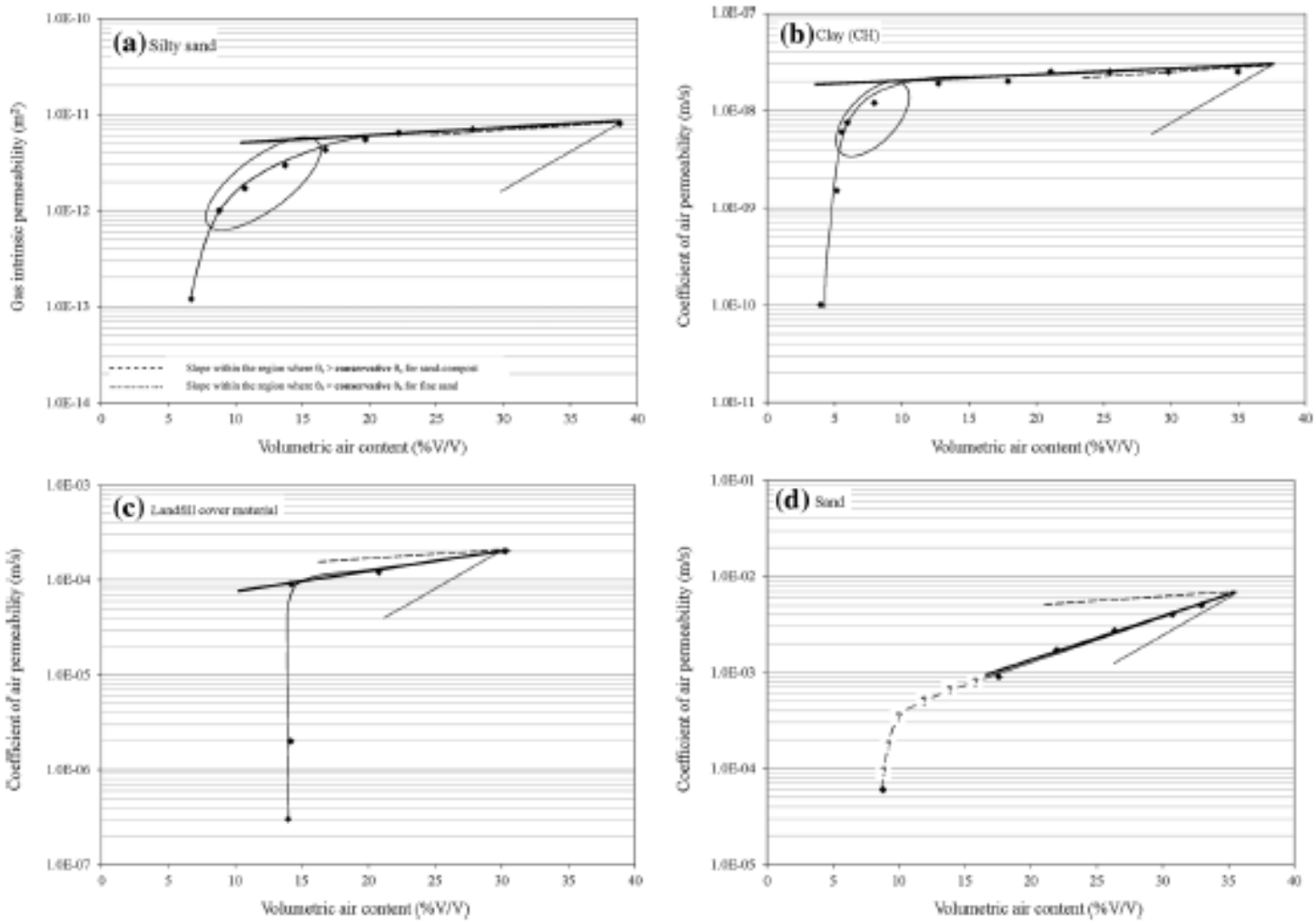

Fig. 8 k_a functions of materials from other studies, adapted from (a) Springer et al. (1998), (b) Jucá and Maciel (2006), (c) Marinho et al. (2001), and (d) Kamiya et al. (2006)

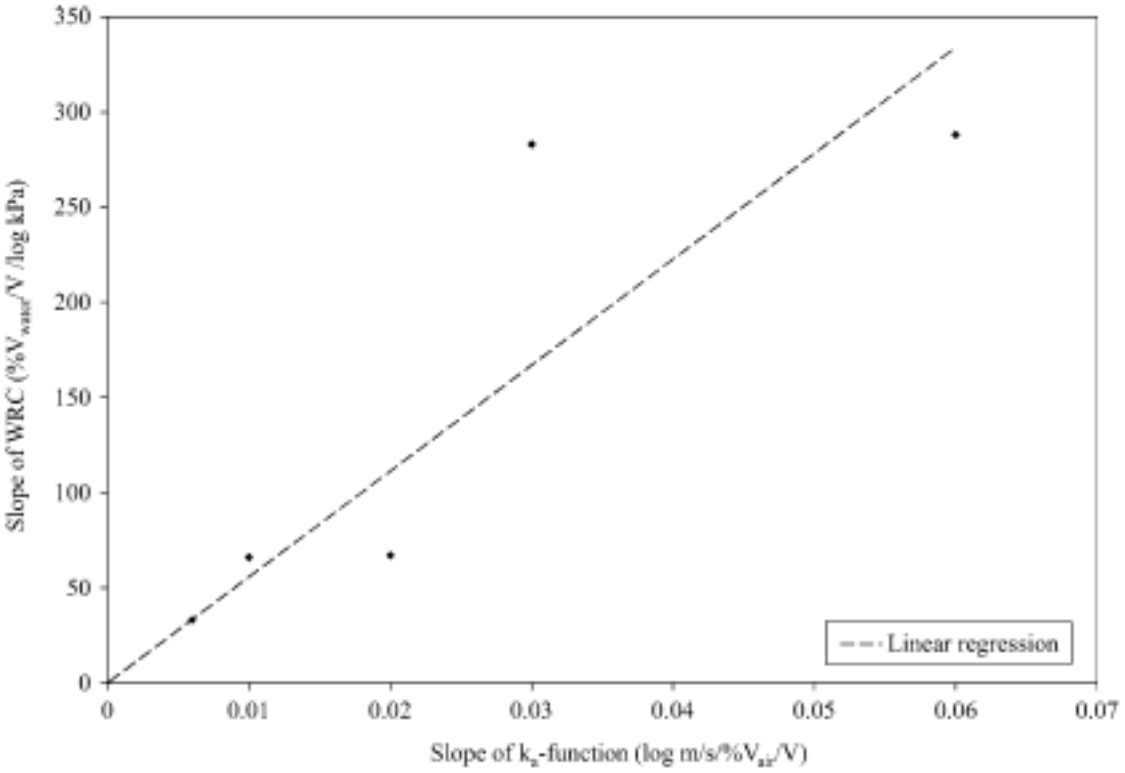

Fig. 9 Relationship between the slope of desaturation zones of WRCs and the slope of k_a-functions for $\theta_a > \theta_{a\text{-}occ}$ or $\theta_a >$ **conservative** $\theta_{a\text{-}occ}$, for materials from other studies and this study

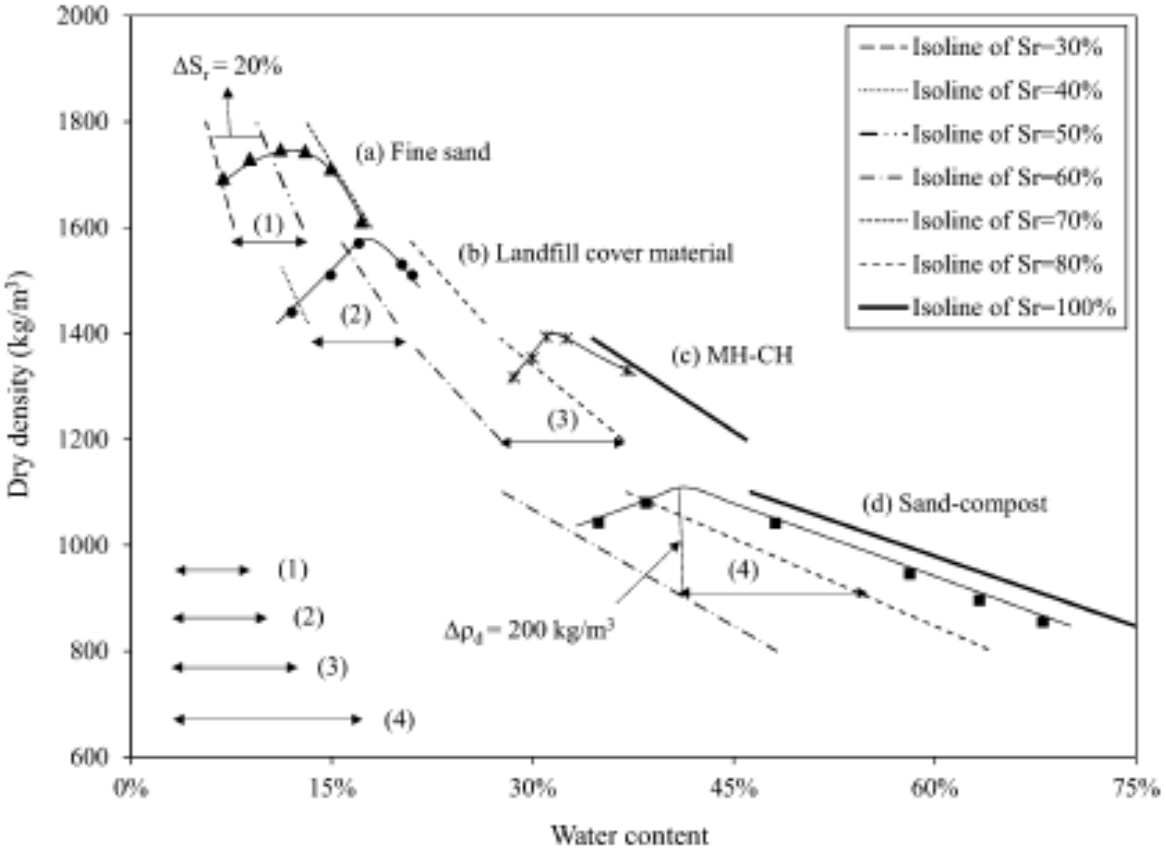

Fig. 10 Compaction curves of (a) fine sand (this study), (b) Landfill cover material adapted from Marinho et al. (2001), (c) MH CH adapted from Langfelder et al. (1968), and (d) sand compost (this study)

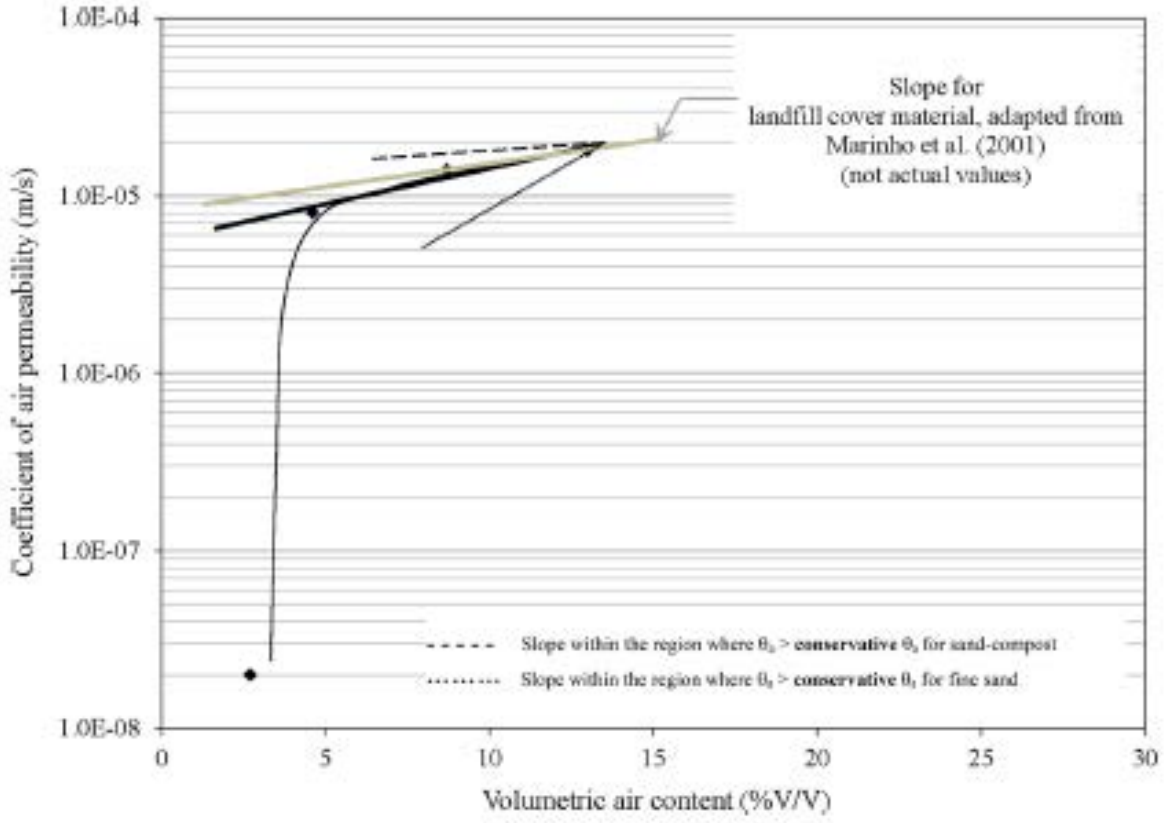

Fig. 11 The k_a function of the MH-CH material adapted from Langfelder et al. (1968), accompanied by materials tested in this study